nature physics

SUPPLEMENTARY INFORMATION
https://doi.org/10.1038/s41567-018-0391-6

In the format provided by the authors and unedited.

Plasmaspheric hiss waves generate a reversed energy spectrum of radiation belt electrons

H. Zhao[1,10*], B. Ni[2,10*], X. Li[1], D. N. Baker[1], W. R. Johnston[3], W. Zhang[2], Z. Xiang[2,1], X. Gu[2], A. N. Jaynes[4], S. G. Kanekal[5], J. B. Blake[6], S. G. Claudepierre[6], M. A. Temerin[7], H. O. Funsten[8], G. D. Reeves[8,9] and A. J. Boyd[9]

[1]Laboratory for Atmospheric and Space Physics, University of Colorado, Boulder, CO, USA. [2]School of Electronic Information, Wuhan University, Wuhan, China. [3]Air Force Research Laboratory, Kirtland Air Force Base, Albuquerque, NM, USA. [4]Department of Physics and Astronomy, University of Iowa, Iowa City, IA, USA. [5]NASA Goddard Space Flight Center, Greenbelt, MD, USA. [6]Space Sciences Department, Aerospace Corporation, Los Angeles, CA, USA. [7]Space Sciences Laboratory, University of California, Berkeley, CA, USA. [8]Los Alamos National Laboratory, Los Alamos, NM, USA. [9]New Mexico Consortium, Los Alamos, NM, USA. [10]These authors contributed equally: H. Zhao, B. Ni. *e-mail: hong.zhao@lasp.colorado.edu; bbni@whu.edu.cn

Supplementary Materials for

Plasmaspheric hiss waves generate a reversed energy spectrum of radiation belt electrons

H. Zhao*, B. Ni*, X. Li, D. N. Baker, W. R. Johnston, W. Zhang, Z. Xiang, X. Gu, A. N. Jaynes, S. G. Kanekal, J. B. Blake, S. G. Claudepierre, M. A. Temerin, H. O. Funsten, G. D. Reeves, and A. J. Boyd

This PDF file includes:

Materials and Methods
Figs. S1 to S10

Materials and Methods

Particle Observations

In this study, the energy spectrum observations are from the Magnetic Electron Ion Spectrometer (MagEIS) and Relativistic Electron and Proton Telescope (REPT) instruments on the Van Allen Probes. NASA's Van Allen Probes, launched on 30 Aug 2012, operate in an elliptical orbit with an inclination of 10° and altitude of ~ 600 km × 5.8 R_E. With the spin axis approximately pointing to the Sun, the spacecraft spins with a period of ~11 s, which provides adequate pitch angle coverage during most times.

MagEIS instruments on Van Allen Probes provide energetic electron flux measurements with an energy range of ~30 - 4000 keV. It contains four independent magnetic electron spectrometers on each spacecraft: one low energy spectrometer, two medium energy spectrometers, and one high energy spectrometer. In this study, we use the electron flux data from low and medium energy units of MagEIS (with an energy range of ~30 - 900 keV). MagEIS electron background-corrected data are preferentially used in our study, for which the contaminations from inner belt protons and bremsstrahlung radiation have been removed[32]; the uncorrected data are only used for the time period when the background-corrected data are unavailable. For MagEIS medium energy units (~230 – 900 keV), background-corrected data are mostly available; for MagEIS low energy units (~30 – 180 keV), at L<4 the background-corrected data are almost always available, while at L>4 mostly uncorrected data are used. It is worth noting that MagEIS high unit data are not used in our study mainly because of its small geometric factor and thus relatively large uncertainties compared to REPT measurements, as well as small calibration differences between MagEIS and REPT instruments. Also, MagEIS high unit on the Van Allen Probes – A can only provide two more energy channels of background-corrected data (~1.6 MeV and ~1.7 MeV) during the studied time periods, which therefore has small influence on our current results.

REPT instruments, each consisting of a stack of silicon solid-state detectors, provide high-quality measurements of relativistic electrons with energy from ~1.8 MeV to >20 MeV. In this study, we use the electron flux data with energies from ~1.8 MeV to ~10 MeV.

The L-shell used in this study is McIlwain L[33] in the Olson and Pfitzer 1977 Quiet (OP77Q) magnetic field model[34].

Bump-On-Tail (BOT) Energy Spectrum: Identification, Characterization, and Uncertainties

An example of bump-on-tail energy spectrum is shown in **Fig. S1** as measured by MagEIS and REPT instruments on the Van Allen Probes – A on 29 March 2015. For a specific energy spectrum, if a flux maximum and a flux minimum can be identified with the corresponding energy of flux maximum greater than that of flux minimum, and the ratio of flux maximum to minimum is greater than 3, then this energy spectrum is identified as a BOT spectrum. **Fig. S1** also shows the electron flux measurements from MagEIS high energy spectrometer (grey cross signs). The agreement between REPT and MagEIS high energy spectrometer is quite good. By defining BOT with flux ratio greater than 3, the small residual calibration difference between MagEIS and REPT electron measurements is unlikely to influence the identification of BOT electron energy spectrum. More detailed cross-calibration between MagEIS and REPT instruments has been done. The results suggest that good agreements between MagEIS and REPT measurements exist at energies ~ 1.8 – 2.6 MeV, and the differences between the measurements of the two instruments are mostly within a factor of 2 – 3. This, again, suggests that this small residual calibration difference between MagEIS and REPT is unlikely to affect the identification of BOT energy spectrum.

The uncertainties in MagEIS and REPT data and their effects on the BOT energy spectra identification are also examined. Fig. S2 shows examples of BOT energy spectra with error bars using data from MagEIS and REPT on the Van Allen Probes – A at three time points on 29 March 2015. It shows that REPT data usually have small uncertainties, while MagEIS data could have large uncertainties when the electron fluxes were low (as those near the flux minimum in BOT energy spectrum). However, note that such uncertainties have little influence on the existence and identification of BOT energy spectra: even including such uncertainties the reversed energy spectra can still be clearly seen. These uncertainties may affect the identification of energy of flux minimum in BOT energy spectrum; however, as shown in Fig. S2, this is unlikely to affect the conclusion that the energy of flux minimum in BOT energy spectrum decreases with increasing L-shell. Thus, though the energy of flux minimum has some uncertainties, our main conclusion about the dependence of energy of flux minimum on L-shell and its consistency with hiss wave scattering remain valid.

Using electron data from the Van Allen Probes – A during the entire year of 2015 and the identification method described above, the occurrence frequency of BOT energy spectra is calculated in grids of 0.1 L-shell and 1 day, and the minimum plasmapause location across all magnetic local times is also calculated using the empirical plasmapause model[11] (**Fig. 2B**). The energy of flux maximum, energy of flux minimum, and the ratio of flux maximum to minimum are also shown in Fig. 2C - 2E. Note that due to an energy gap in our energy spectra (~1 – 1.8 MeV), the energy of flux maximum is mostly identified to be 1.8 MeV; however, the actual energy of flux maximum could be somewhere between 1 and 1.8 MeV though the energy resolution in the data is not high enough to clearly show it. Similarly, the ratio of flux maximum to minimum also has some uncertainties due to the energy resolution as well as the small calibration difference between MagEIS and REPT instruments, but the uncertainties are expected to be small and probably indiscernible in Fig. 2E since the plot is in logarithm scale.

The statistics of BOT energy spectra during the year of 2016 and 2017 is also shown in Fig. S3 and S4. Compared to the year of 2015, during 2016 and 2017 more geomagnetic storms were driven by the corotating interaction regions (CIR) rather than coronal mass injections (CME), while the BOT energy spectrum is still the most prevalent type of energy spectra inside the plasmasphere at L>~2.6 regardless of the solar wind driver. And the characteristics of BOT energy spectra in 2016 and 2017 are quite similar to those in 2015: the energies of flux maximum and minimum are higher at lower L-shells, consistent with the hiss wave scattering, and the ratio of flux maximum to minimum is ~ 10 – 100.

Note that though the main results we showed in Fig. 1 and 2 are based on spin-averaged electron fluxes, the BOT energy spectra actually exist for electrons with a wide range of equatorial pitch angles. Fig. S5 shows the energy spectra evolution of electrons with equatorial pitch angles of 30° and 60° at L=3.0, 3.5, and 4.0 during 20 – 30 March 2015, using pitch-angle-resolved data from the Van Allen Probes – A and mapping the observations to the geomagnetic equator using OP77Q model. It clearly shows that the BOT energy spectra generally exist for electrons with different equatorial pitch angles.

Phase Space Density Spectrum on March 29, 2015

The bump-on-tail (BOT) energy spectra developed inside the plasmasphere during the recovery phase of March 2015 storm (**Fig. 1, F to H**). We also calculate the electron phase space densities (PSD) using OP77Q magnetic field model during this time period and examine them at four fixed pairs of the second and third adiabatic invariants (i.e., K and L^*) as a function of the first adiabatic invariant μ. During this time period the electron PSD spectrum also showed the BOT feature (**Fig. S6**): given values of K and L^*, the electron PSD spectrum has a minimum around μ

= 10s – ~100 MeV/G and a maximum around several hundreds of MeV/G. Compared to the BOT energy spectrum, the ratio of PSD maximum to minimum is relatively smaller, and the L range of observed BOT feature is also narrower. These results indicate that the BOT feature not only exists in the electron energy spectrum but also in the electron PSD profile. The electron PSD spectra with a wider K range at 22:00 UT on 29 March 2015 are also examined (Fig. S7), and the results suggest that the BOT feature clearly exist in the electron PSD spectrum with a wide K range inside the plasmasphere, and the μ values of the flux maximum and minimum decrease as K increases.

Wave Model of Plasmaspheric Hiss

In order to develop a reasonable wave model of plasmaspheric hiss for the 10-day period of 20 – 30 March 2015, we focus on the three specific L-shell ranges, i.e., L = 3.0 ± 0.1, 3.5 ± 0.1, and 4.0 ± 0.1, for both inbound and outbound spacecraft trajectories. An event of hiss emissions is identified by applying the criterion of right-handed polarization with the ellipticity > 0.9, wave frequencies between 50 Hz and 2 kHz, and its location below the plasmapause inferred from the traces of upper hybrid resonance frequency. The identified wave spectral intensities are then averaged for adoption as the representative profile of hiss spectral intensity for each L-shell range during the corresponding half orbit. The mean profile is also used to calculate the average hiss wave amplitude by integrating the wave spectral intensity over frequency. In doing so, we acquire a time-varying, data-driven model of plasmaspheric hiss wave spectral intensity and wave amplitude (**Fig. 3C**).

Hiss-Induced Electron Scattering Rates

Since the hiss wave spectral intensity variations are relatively small, their mean profiles provide a good representation of the general spectral features of plasmaspheric hiss during the considered half orbit. Under the assumption that the wave spectral intensity remains unchanged with latitude, the data-driven mean profiles of plasmaspheric hiss spectral intensity are subsequently adopted as inputs to evaluate hiss wave induced rates of electron scattering. To evaluate wave-induced electron diffusion coefficients, the distribution of wave normal angle as a function of latitude is another critical parameter required for numerical computations. We follow previous studies[17-21,26] to adopt a Gaussian distribution given by $g(X) = \exp[-(X - X_m)^2/(\delta X)^2]$ $(X_{lc} \leq X \leq X_{uc})$, where $X = \tan(\theta)$ with θ as the wave normal angle, δX (= $\tan(\delta\theta)$) is the angular width,

X_m (= tan(θ_m)) is the peak, X_{lc} (=tan(θ_{lc})) and X_{uc} (=tan(θ_{uc})) are the lower and upper bounds of the wave normal distribution outside which the wave power is zero. To evaluate the hiss induced bounce-averaged electron scattering rates, the detailed information of wave normal angle distribution over the electron bounce trajectory along one specific field line (in this study, say, L = 3.0, 3.5, and 4.0) is required. More specifically, the values of four input parameters, i.e., θ_m, $\delta\theta$, θ_{lc} and θ_{uc}, are required as functions of geomagnetic latitude, which, however, cannot be directly derived from in situ observations. In addition, while the satellite data can be analyzed to acquire the values of wave normal angle as a function of wave frequency (which can be taken as the peak wave normal angle θ_m), the measurements cannot provide the other information of wave normal angle distribution, say, $\delta\theta$, θ_{lc} and θ_{uc}. Therefore, reasonable assumptions are consequently required to facilitate the simulation runs. We follow a previous study[18] to adopt the model of hiss wave normal angle distribution as a function of latitude.

The dipolar geomagnetic field model is used in our calculations with its equatorial magnitude derived from the spacecraft measurements. In other words, this is a "scaled" dipole magnetic field by the measured magnetic field magnitude to make the simulation closer to the real situation. During each considered time interval, the ambient electron densities are acquired from the EMFISIS high frequency receiver upper hybrid resonance frequencies. Then we take the averaged density values for each period as inputs, along with the assumption of latitudinally constant density model. With all the above information available, we evaluate the quasi-linear bounce-averaged electron diffusion coefficients by plasmaspheric hiss, for which the resonance harmonics $|N| \leq 5$ are considered. The diffusion rate calculations are implemented for each considered L-shell during both inbound and outbound intervals. **Fig. S8** shows an example of hiss-induced rates of electron pitch angle diffusion, cross diffusion and momentum diffusion as a function of equatorial pitch angle and electron kinetic energy at L = 3.0, 3.5, and 4.0 during the interval of 21:27 - 22:02 UT on 25 March 2015.

<u>Simulation Results of Energy Spectra Evolution of Electrons with Various Equatorial Pitch Angles</u>

Based upon the numerical results of our 2-D Fokker-Planck diffusion simulations at three specific L-shells, i.e., L = 3.0, 3.5, and 4.0, we also investigate the temporal evolution of energy spectra for outer radiation belt electrons at equatorial pitch angles away from 90°, which are shown in Fig. S9. Under the impact of hiss wave scattering, the BOT spectral features form clearly for all the two considered equatorial pitch angles (i.e., 30° and 60°), which is consistent with our observations, indicating that the production of BOT spectrum is very likely a process for electrons at all pitch angles. Compared to the results for equatorially mirroring electrons (Fig. 4), the electron energies of BOT flux minima tend to be very similar for all considered equatorial pitch angles. However, the timings and detailed profiles of the evolution of BOT electron energy spectra differ considerably at different L-shells, which can be primarily attributed to the L-shell dependence of the hiss-induced electron scattering effect.

Sensitivity of 2-D Fokker-Planck Simulation Results

In order to perform the 2-D diffusion simulations, a number of assumptions have been made regarding the input parameters including the latitudinal variations of wave spectral intensity and wave normal angle distribution and the profiles of ambient magnetic field and plasma density. To explore the sensitivity of our model results to several key input parameters and consequently the dependence of the evolution of BOT electron energy spectrum on our adopted assumptions, we implement further numerical runs of 2-D Fokker-Planck diffusion simulations to seek for a preliminary parametric analysis. We first select a set of input parameters as the standard, and then vary one input parameter but keep the other unchanged to investigate the sensitivity of the model results to the specific parameter. The standard of input parameters are adopted as follows: the exact dipole geomagnetic field model, the latitudinally constant plasmaspheric density model of Sheeley et al.[35], the latitudinally varying model of wave normal angle distribution from Ni et al.[18], the Gaussian frequency spectrum of hiss between 100 Hz and 2 kHz with the peak frequency of 300 Hz and the bandwidth of 550 Hz[17,18], the constant wave amplitude of 30 pT, and the latitudinal confinement within 40° of the geomagnetic equator. From left to right, Fig. S10 displays the 2-D plots of hiss-induced bounce-averaged electron pitch angle diffusion, cross diffusion and momentum diffusion as a function of equatorial pitch angle and electron kinetic energy and the model results of corresponding 10-day evolution of the equatorially mirroring electron energy spectra at L= 3.5. For top to bottom, the results correspond to the standard set of input parameter, low frequency hiss spectrum, increase and decrease of the ambient plasma density by a factor of 2, increase and decrease of the background magnetic field by a factor of 2, and small (quasi-parallel) wave normal angle distribution with $\theta_{lc} = 0°$, $\theta_{uc} = 45°$, $\theta_m = 0°$ and $\delta\theta = 30°$. Overall, changes of the background magnetic field can introduce largest variations in the evolution of BOT electron energy spectrum. In contrast, the BOT spectral features are less sensitive to the variations of wave frequency spectrum, ambient plasma density and wave normal angle distribution, while these changes also modify the temporal profiles of the BOT electron energy spectrum.

References

32. Claudepierre, S. G., T. P. O'Brien, J. B. Blake, J. F. Fennell, J. L. Roeder, J. H. Clemmons, M. D. Looper, J. E. Mazur, T. M. Mulligan, H. E. Spence, et al., A background correction algorithm for Van Allen Probes MagEIS electron flux measurements, J. Geophys. Res. Space Physics, 120, 5,703-5,727, 2015.

33. McIlwain, C. E., Coordinates for mapping the distribution of magnetically trapped particles, J. Geophys. Res., 66(11), 3,681–3,691, 1961.

34. Olson, W. P., and K. Pfitzer, Magnetospheric magnetic field modeling, Annu. Sci. Rep. F44620-75-c-0033, Air Force Off. of Sci. Res., Washington, D. C, 1977.

35. Sheeley, B. W., M. B. Moldwin, H. K. Rassoul, and R. R. Anderson, An empirical plasmasphere and trough density model: CRRES observations, J. Geophys. Res., 106, 25,631-25,641, 2001.

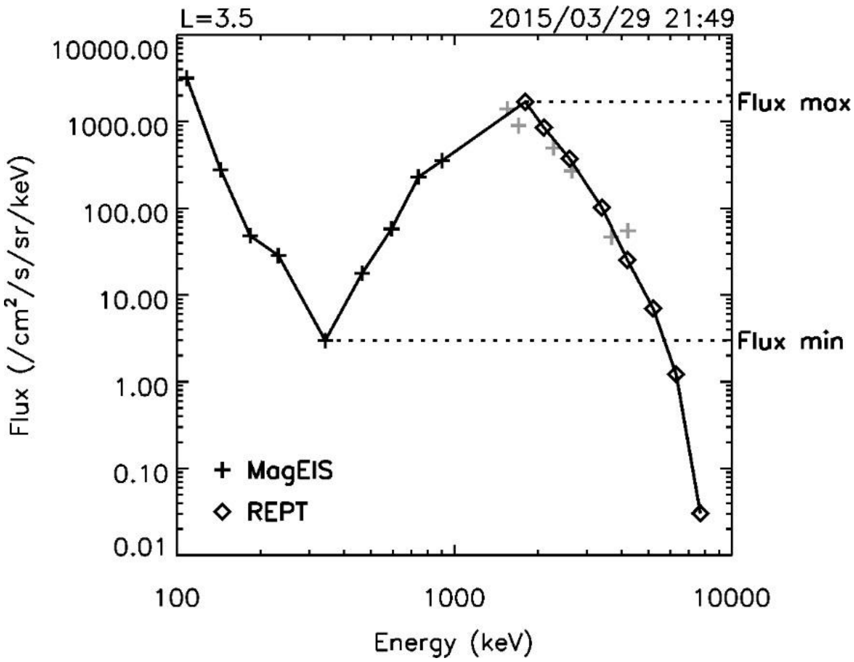

Fig. S1. An example of bump-on-tail energy spectrum at L=3.5, measured by the Van Allen Probes – A at 21:49 on 29 March 2015. Black cross signs represent data from MagEIS instruments, and diamond signs represent data from REPT instruments. The grey cross signs show data from MagEIS high energy spectrometer. Flux maximum and minimum of this BOT spectrum are also identified in the figure.

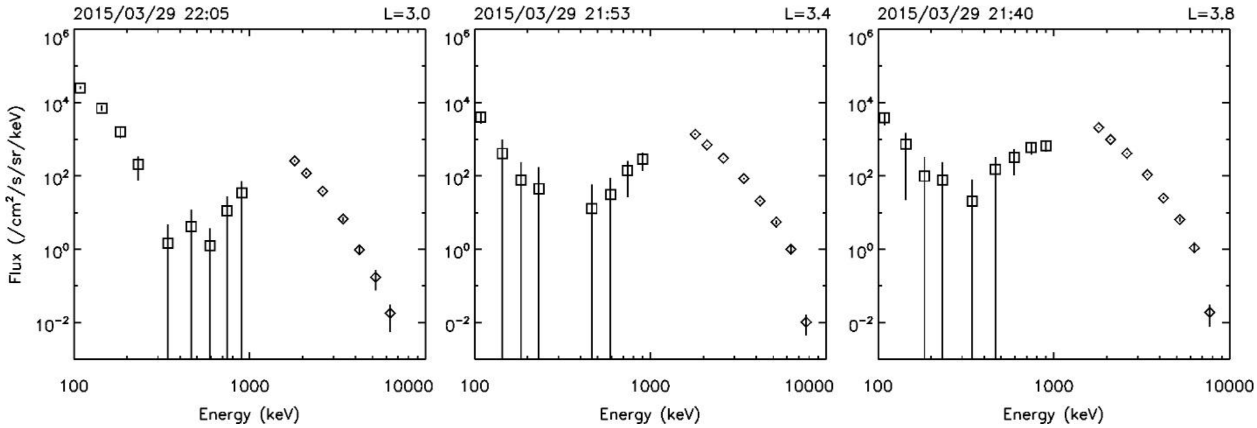

Fig. S2. Radiation belt electron bump-on-tail energy spectra with error bars using data from MagEIS and REPT instruments on the Van Allen Probes – A at three time points on 29 March 2015.

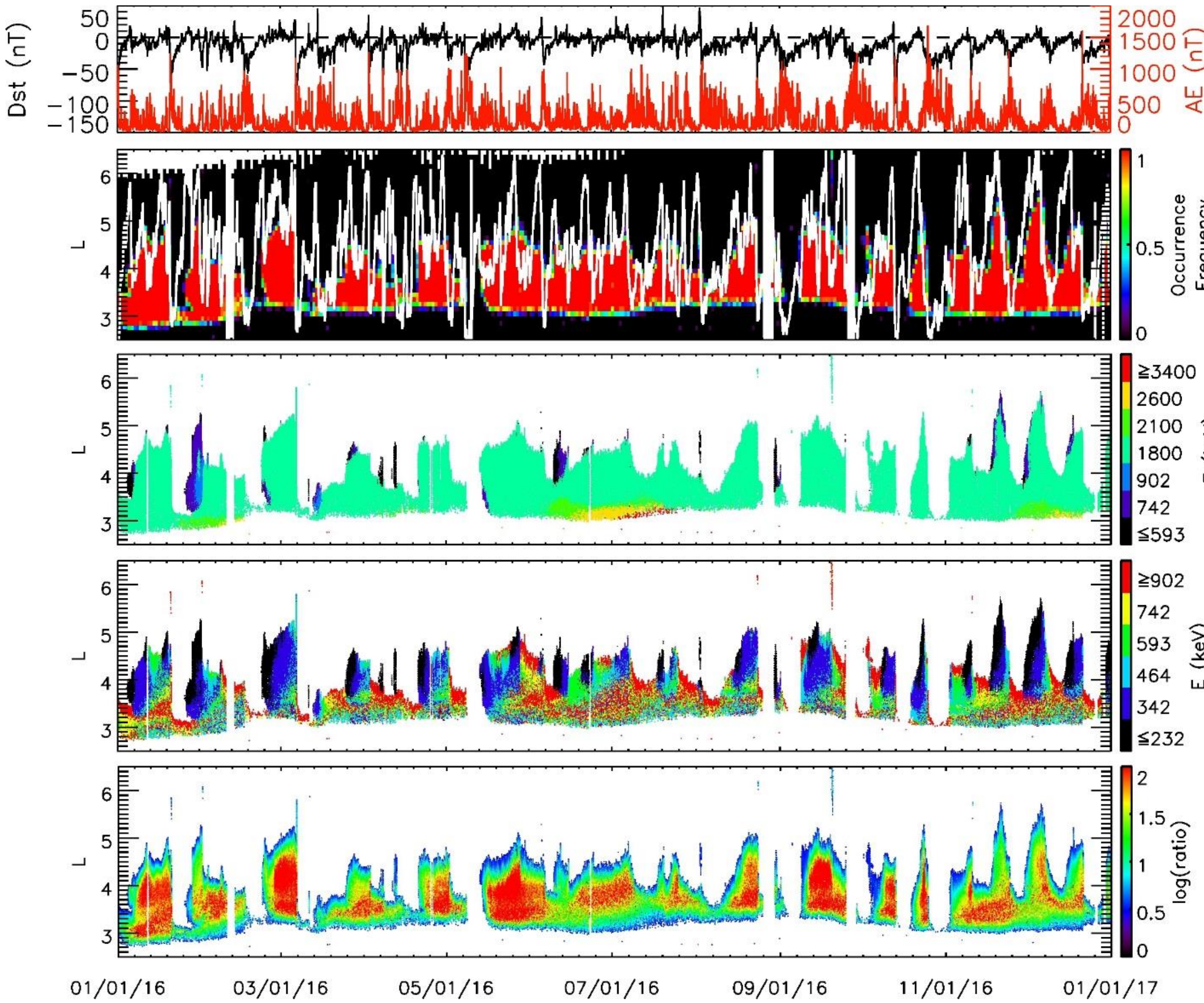

Fig. S3. Statistics of bump-on-tail (BOT) electron energy spectrum based on the Van Allen Probes – A's measurements during 2016. The format is the same to that in Fig. 2.

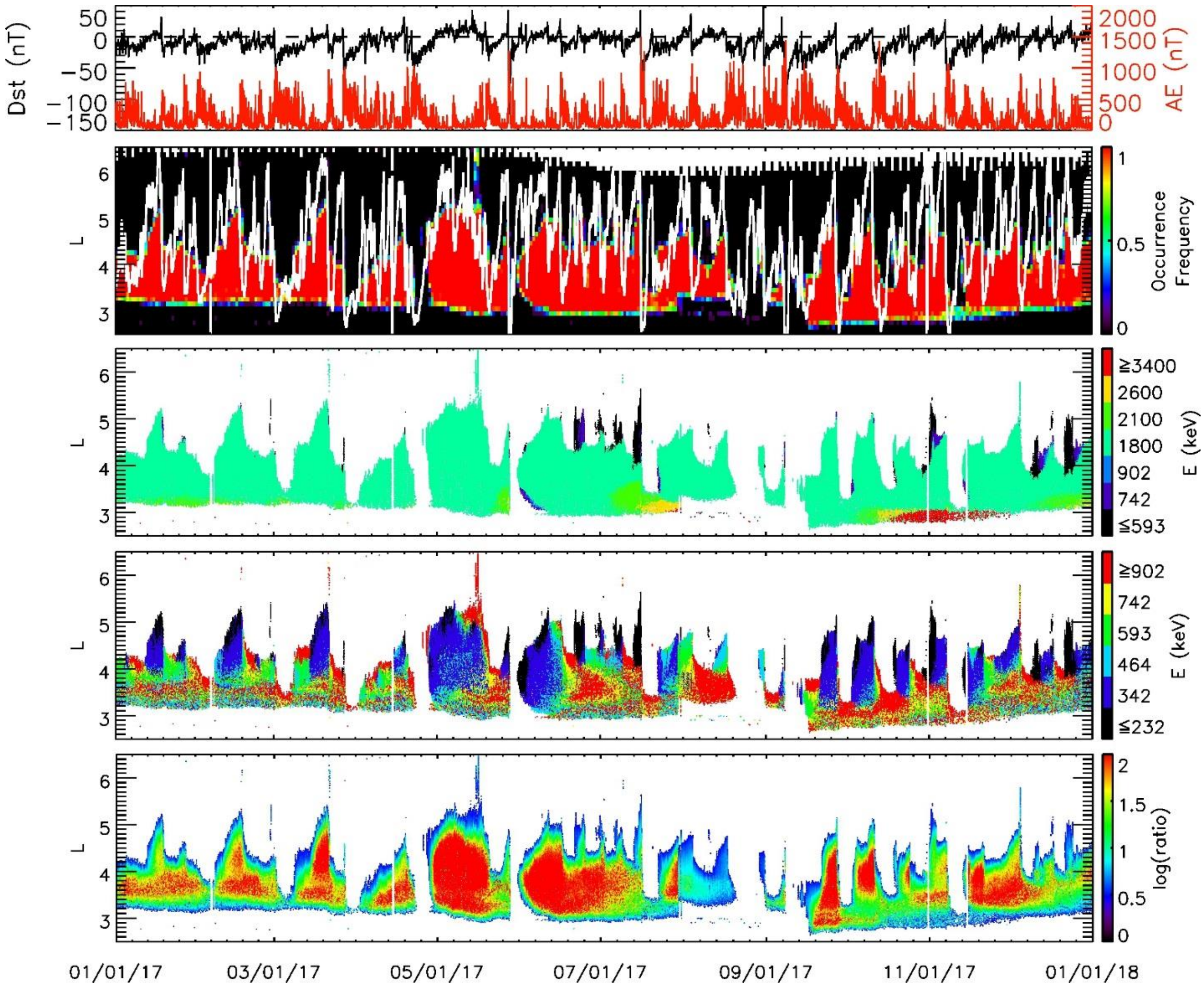

Fig. S4. Statistics of bump-on-tail (BOT) electron energy spectrum based on the Van Allen Probes – A's measurements during 2017. The format is the same to that in Fig. 2.

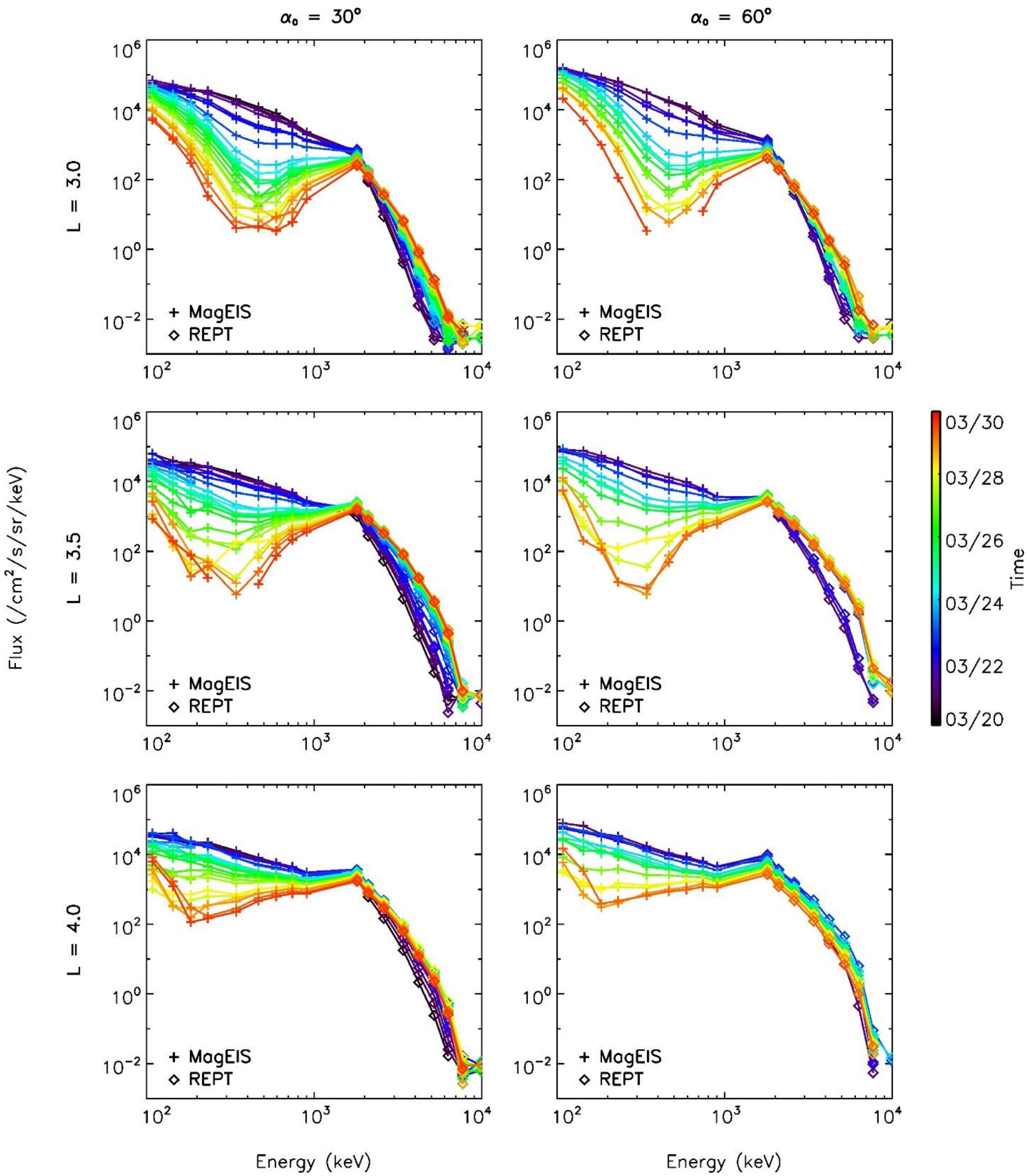

Fig. S5. Evolution of the energy spectra of electrons with equatorial pitch angles of (left) 30° and (right) 60° at (top) L=3.0, (middle) 4.0, and (bottom) 5.0 during 20 – 30 March 2015, using data from the Van Allen Probes – A.

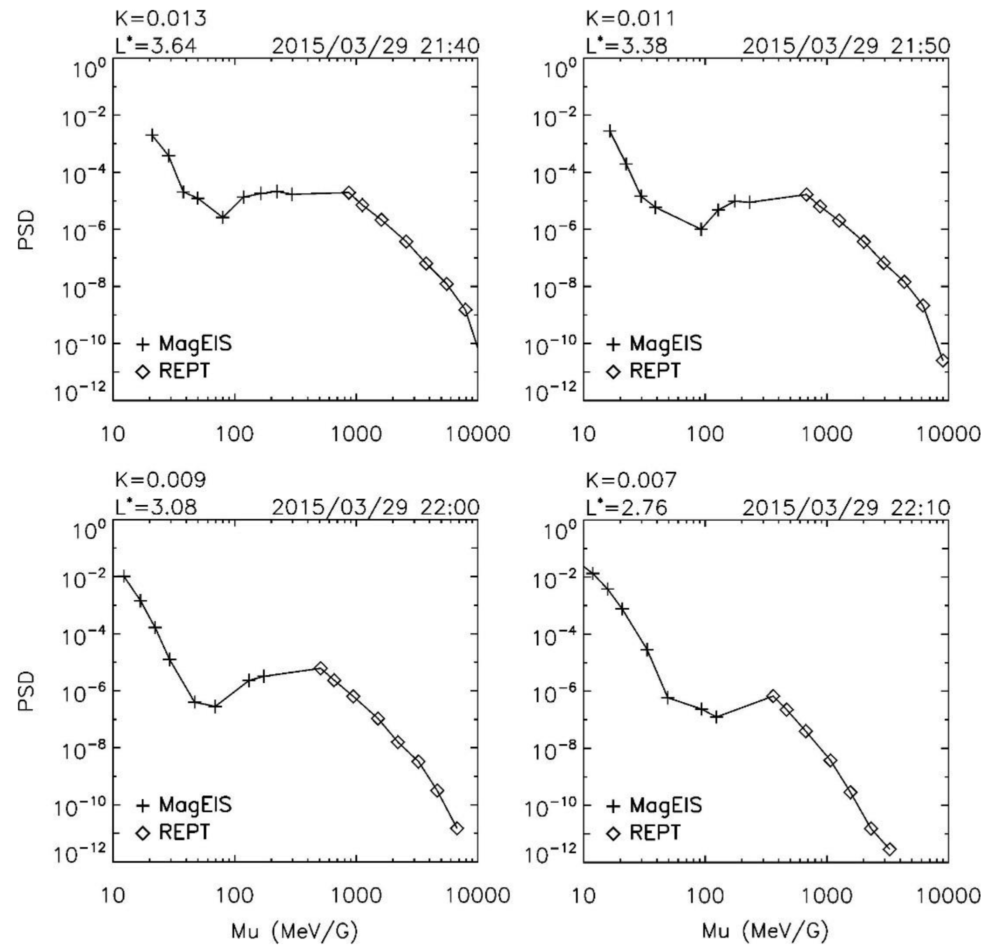

Fig. S6. Calculated electron phase space densities (PSD) using OP77Q magnetic field model at the four fixed pairs of the second and third adiabatic invariants (i.e., K and L*) as a function of the first adiabatic invariant μ during the time interval of 21:40 – 22:10 UT on 29 March 2015. The BOT feature is also clearly present in the electron PSD profile.

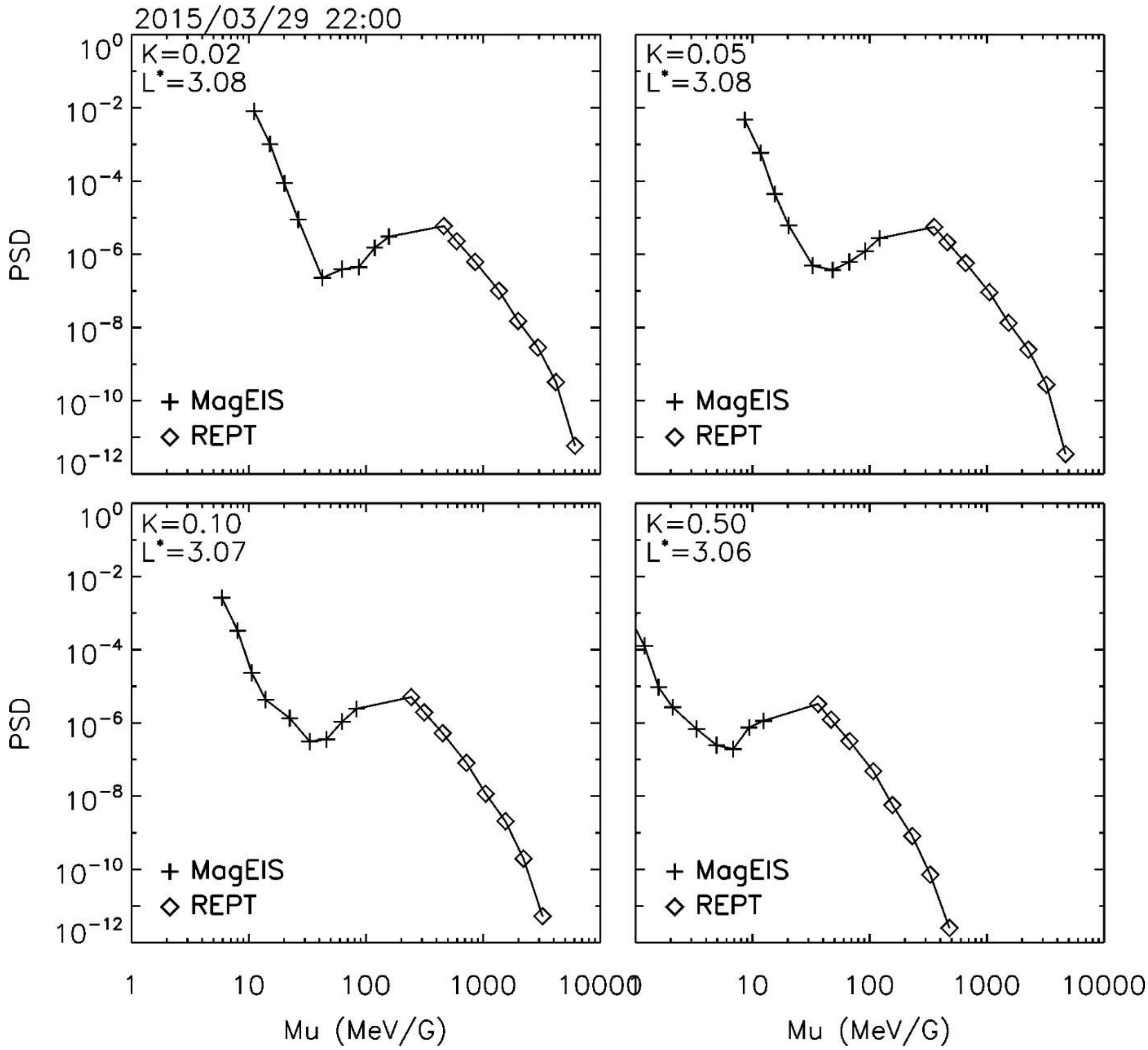

Fig. S7. Calculated phase space densities using OP77Q magnetic field model for the four fixed pairs of K and L^* as a function of μ at 22:00 UT on 29 March 2015. The BOT feature is clearly present in these PSD profiles with a wide K range.

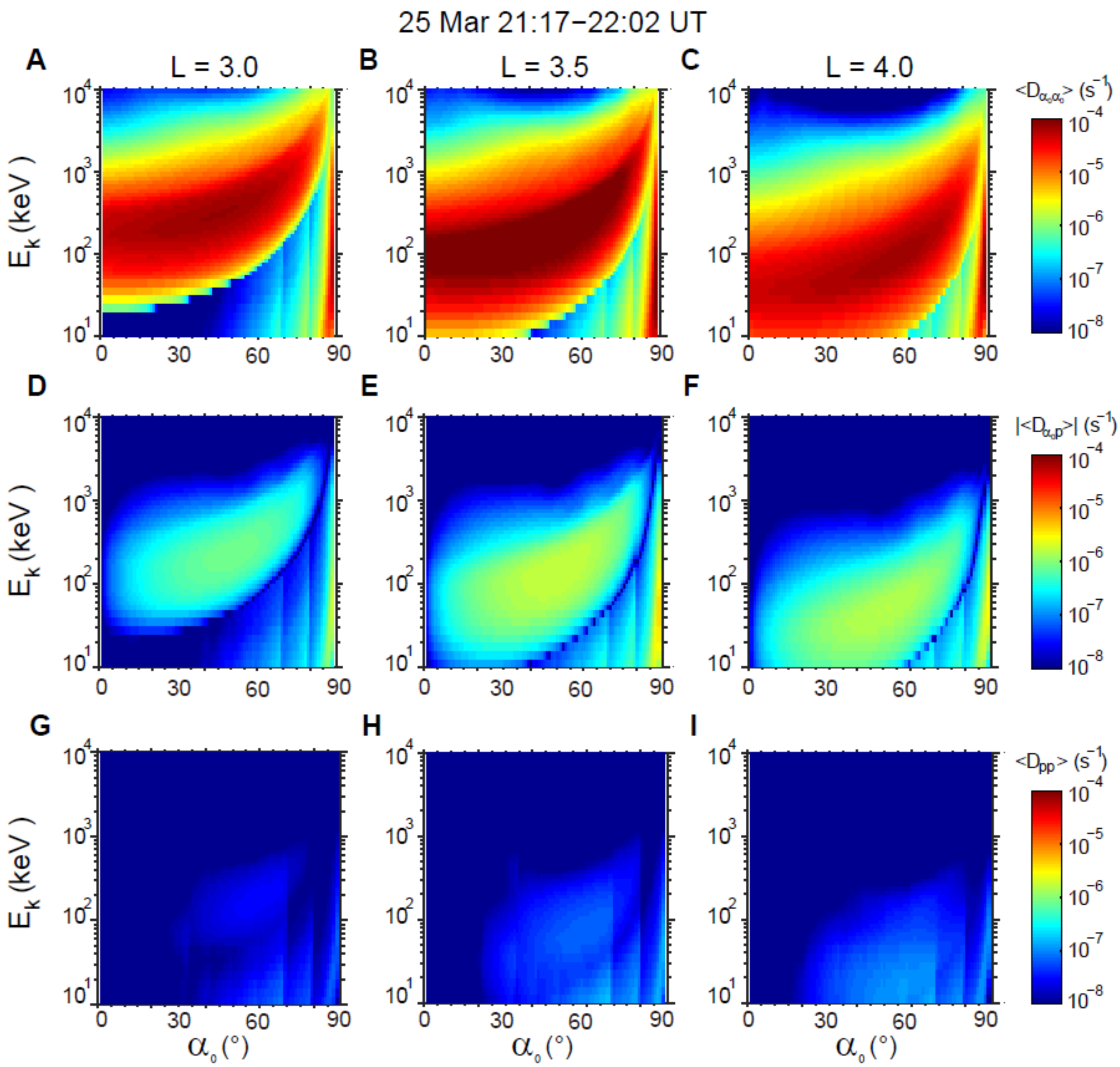

Fig. S8. An example of 2-D plots of hiss-induced rates of electron pitch angle diffusion, cross diffusion and momentum diffusion as a function of equatorial pitch angle and electron kinetic energy at L = 3.0, 3.5, and 4.0 during the interval of 21:27 - 22:02 UT on 25 March 2015.

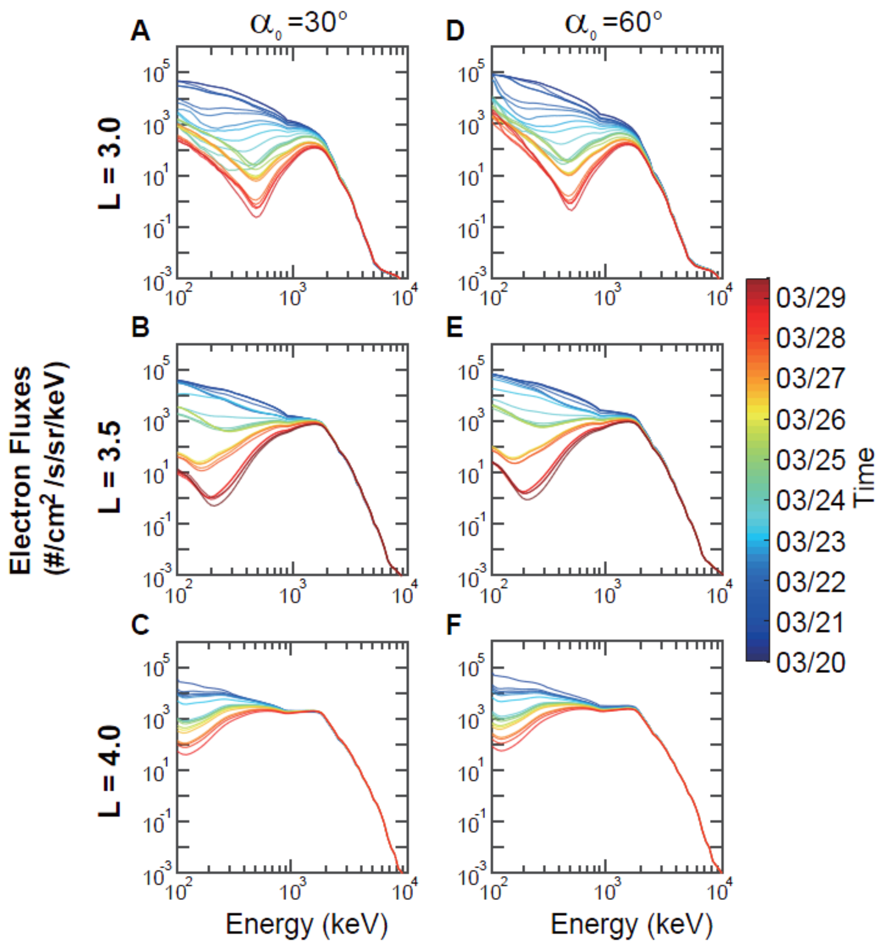

Fig. S9. Simulated temporal evolution of energy spectra for outer radiation belt electrons at two equatorial pitch angles: (left) 30° and (right) 60°, and three specific L-shells: (from top to bottom) L = 3.0, 3.5, and 4.0. Under the impact of hiss wave scattering, the BOT spectral features form clearly for all considered equatorial pitch angles, indicating that the production of BOT spectrum is very likely a process for electrons at all pitch angles.

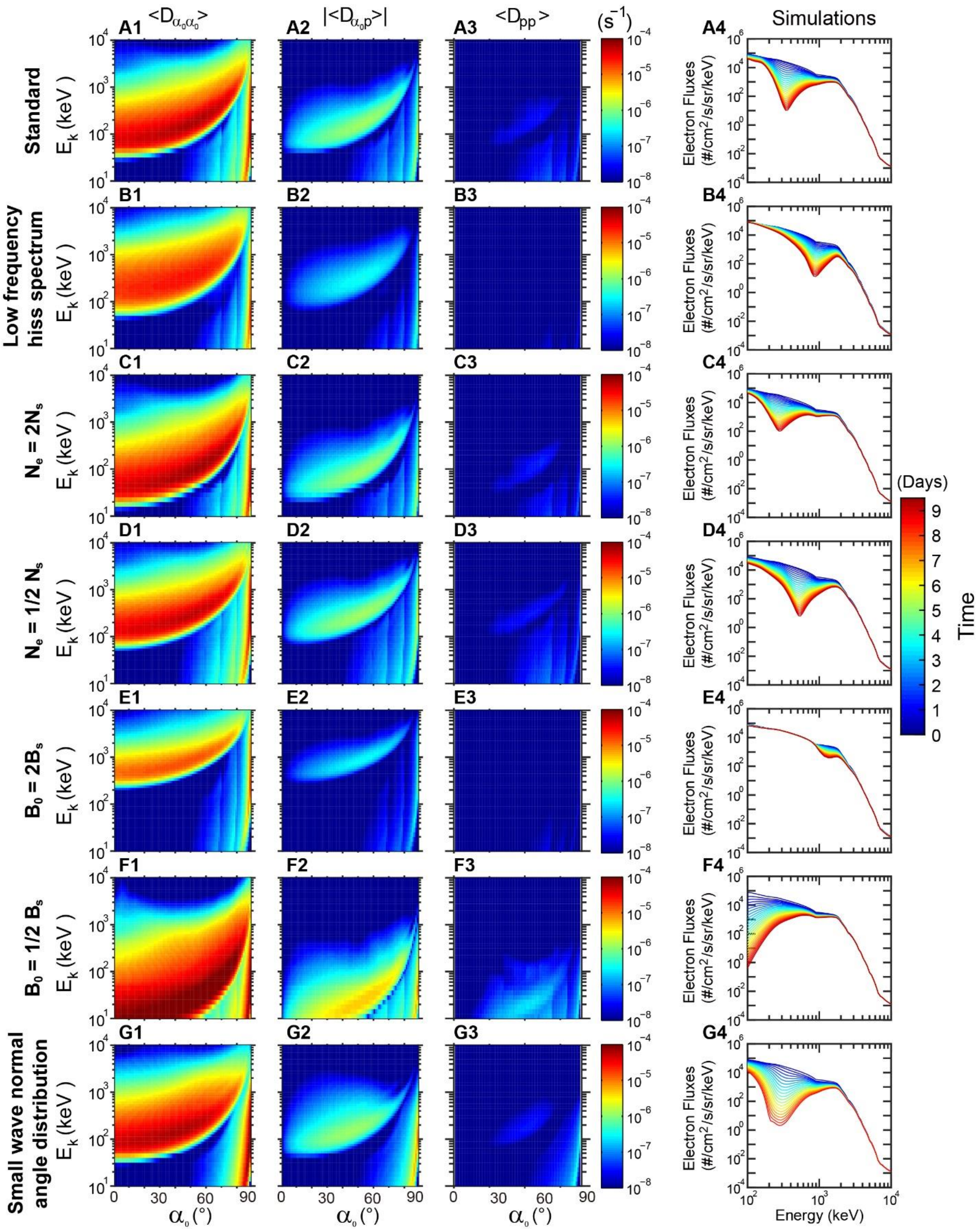

Fig. S10. (from left to right) 2-D plots of hiss-induced bounce-averaged electron pitch angle diffusion, cross diffusion and momentum diffusion as a function of equatorial pitch angle and electron kinetic energy, and the model results of evolution of the equatorially mirroring electron energy spectra at L= 3.5 during 20 – 30 March 2015 for different sets of input parameters. From top to bottom, the results show using the standard set of input parameter, low frequency hiss spectrum, increase and decrease of the ambient plasma density by a factor of 2, increase and decrease of the background magnetic field by a factor of 2, and small (quasi-parallel) wave normal angle distribution with $\theta lc = 0°$, $\theta uc = 45°$, $\theta m = 0°$ and $\delta\theta = 30°$, respectively. These results show the dependence of the formation and evolution of BOT electron energy spectrum on the variations of background magnetic field, wave frequency spectrum, ambient plasma density, and wave normal angle distribution.